Microgravity Science and Technology (2019) 31:31–48
https://doi.org/10.1007/s12217-018-9662-1

ORIGINAL ARTICLE

Design of an Active Disturbance Rejection Control for Drag-Free Satellite

Chu Zhang [1,2] · Jianwu He [1,2] · Li Duan [1,2] · Qi Kang [1,2]

Received: 19 January 2018 / Accepted: 15 October 2018 / Published online: 10 November 2018

Abstract
This paper addresses the problem of designing an active disturbance rejection controller for a high accuracy drag-free satellite with cubic test mass. The uncertain model of the drag-free satellite is defined. The performance requirement imposed on the acceleration of the test mass is broken down into specification of drag-free and suspension loop because of the disturbance decoupling controller, which is based on the linear active disturbance rejection control technique. We derive two-degree internal model control structure of ADRC, which is used for robust stability verification. Search programs determine the parameters that satisfy system stability and the performance requirement. The design technique has shown to be robust to the perturbation of the system and good performance in disturbance suppressing. To check the design of the controller, an overall simulation is preformed, and the results confirmed that the controller is able to meet the system requirements.

Keywords Spacecraft · Drag-free control · Active disturbance rejection control · Disturbance decouple

Introduction

In recent years, drag-free satellites (Lange 1964; DeBra 1997; Armano et al. 2016) have played key roles in many space science projects, including navigation, earth science, fundamental physics, and astrophysics. In the area of navigation, the drag-free satellites have been used for autonomous fuel-efficient orbit maintenance, and precision real-time onboard navigation (Leitner 2003). In geodesy applications, the drag-free satellites allow for the fine-structured gravity field maps of the Earth (Carraz et al. 2014). For example, the GOCE satellite (Canuto 2008) that is launched in 2009, is part of the European space program dedicated to exploring the Earth's gravity field. Scientists have also explored drag-free satellites that are simple and cost-effective for autonomous observations of Earth, as well as in Earth atmospheric studies (Nguyen and Conklin 2015). In fundamental physics, the drag-free satellites have been used for equivalence principle testing, including the Microscope mini-satellite (Touboul et al. 2002), operated by the CNES, which is used to test the universality of equivalence principle with a precision to the order of 10^{-15}, 100 times more precise than could be achieved on Earth. It was launched in 2016. In the area of astrophysics, drag-free technology is key to LISA Pathfinder (Fichter 2005a, Armano et al. 2016), which tests the technologies needed for the Laser Interferometer Space Antenna (LISA). The LISA is a European Space Agency mission designed to detect and accurately measure gravitational waves, which is planned to be launched in 2030 *s. China* has also propose space gravitational wave detection and earth gravity mapping projects based on drag-free technology (Li et al. 2018).

The drag-free satellites are equipped with gravitational reference sensors (GRS), which shield a free-flying test mass (TM), also referred as proof mass, both from external disturbances and disturbances caused by the satellite itself. The GRS measures the position and attitude of the test mass with

This article belongs to the Topical Collection: Approaching the Chinese Space Station - Microgravity Research in China
Guest Editors: Jian-Fu Zhao, Shuang-Feng Wang

✉ Qi Kang
kq@imech.ac.cn

Chu Zhang
zhangchu@imech.ac.cn

Jianwu He
javehe@imech.ac.cn

Li Duan
duanli@imech.ac.cn

[1] Institute of Mechanics, Chinese Academy of Sciences, 100190 Beijing, People's Republic of China

[2] School of Engineering Science, University of Chinese Academy of Sciences, Beijing 100190, People's Republic of China

respect to the spacecraft, and a feedback control system commands high precision continuous thrusters to keep the satellite centered within the test mass. Typically, for the cubic test mass or more than one test mass within a satellite, an electrostatic suspension actuator is required to control the position and attitude of the test mass with respect to the satellite. The drag-free performance requirements are usually specified as residual acceleration noise spectral densities of the test mass or masses along a specific axis.

Because of the dynamic coupling and relative motion between the test mass and spacecraft, it has proven to be very challenging to achieve the requirements imposed by the scientific goals. There are many related studies conducted regarding this problem (Fichter et al. 2005a, b, 2006, Bortoluzzi et al. 2003, 2004, Chapman et al. 2002). The couplings among the different degrees of freedom are decoupled by the feedback interconnections between the overall systems, which yield a system of decoupled simple single-input to single-output (SISO) systems. Control synthesis methods have been used to design controllers for these SISO systems. These have included a proportional- integral-derivative (PID) (Chapman et al. 2002), and optimization based on the definition of a weight function (Bortoluzzi et al. 2003, 2004), as well as $\mathcal{H}_\infty$ synthesis techniques (Fichter et al. 2005a, b, 2006). In all of these cases, the structural uncertainties of the design plants are not taken into consideration. On the other hand, the robust drag-free controller synthesis method that is proposed by Pettazzi et al. (2009), in which the ν-gap metric is used to derive a simplified uncertain design plant, along with the control design technique based on mixed structure singular value, is used to synthesize a SISO controller. However, the decoupling method is approximate, and the controller of this synthesis technique is complex. Moreover, it has been found that the robust control synthesis is usually conservative, at the cost of the systems' performances.

When considering the problem of drag-free control in this paper, a disturbance rejection based approach has been proposed to synthesis the controller (Zheng et al. 2009). The cross-couplings between the different control loops, as well as the external disturbances, have been treated as total "disturbance" estimated and rejected in real time. This strategy originated from the active disturbance rejection control (Han 2009), which is less dependent on the model due to its idea of using an extended state observer (ESO) to estimate the total "disturbance", which includes both the internal disturbances and the external disturbances of the plant. The ADRC displays strong robustness and outstanding performances in the application research results (Xia et al. 2011, Liu and Li 2012). The objective of this study is to design a controller which could decouple the system, and also exhibit good performances in the parameter uncertainties and disturbance rejections.

The contributions of this work are in following aspects:

(1) We develop disturbance decoupling control based on ADRC, and transform it into the form of transfer function, the control structure is simpler than that of (Zheng et al. 2009);
(2) We derive two degree structure internal model control structure of ADRC based on reduce extend state observer, based on this the robust stability condition of the controller is derived, which is used to the robust stability verification;
(3) We derive the search algorithm based on stability criteria and performance requirement conditions to determine controller parameters.

This paper is organized as follows: Section 1 is the introduction; In Section 2, the design model of the drag-free satellite is presented; In Section 3, the decoupling method, which is based on active disturbance rejection control and a disturbance rejection controller designed for the system, is detailed; In Section 4, the design results of this controller are presented; and finally, the conclusion is presented in Section 5.

Mathematical Model of the Drag-Free Satellite

This section presents a drag-free satellite model with a cubic test mass. Stephen Theil (2002) and Pettazzi (2008) have derived the system dynamics. In this model, the satellite is placed in the Sun-Earth Lagrangian point. The force and torque acting on the spacecraft due to drag-free control is provided by means of micro-thrusters (Gollor and Franke 2016), which are modeled as a first order system. The time constant takes into account the delays introduced by the electronic devices which driving the thrusting actuators. However, in past research, the delay of the suspension actuator front-end electronic (FEE) (Li et al. 2011) has not been considered, and this parameter definitely affected the designed controller. In this research, the FEE is also modeled as a first order system. In this section, we will briefly introduce the system dynamics of drag-free satellite, more details can be found in (Pettazzi 2008).

The simplified block-diagram of satellite system is shown in Fig. 1, and the reference frames, which are relevant for the derivation of the equation of motion, are depicted. In this figure, $\sum I$ denotes the inertial coordinate system; $\sum SC$ is the spacecraft body reference, and $\sum TM$ is the body reference frame of the test mass.

As derived by Pettazzi (2008), the linearized equations describing the motion of the test mass with respect to the spacecraft are

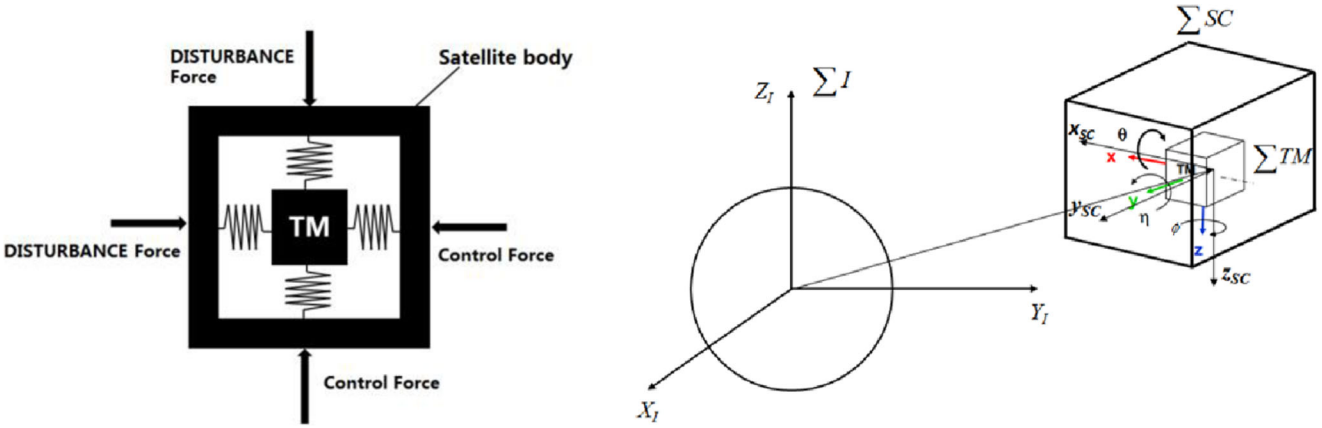

Fig. 1 Schematic of drag-free satellite with its test mass

$$\ddot{q} = M_q^{-1}\{Kq + f_{SUS} + f_{TM} + (M_u M_{SC}^{-1})(f_{dist} + f_{DF})\} \quad (1)$$

$$f_{SUS} = (I + H_{IS})F_{SUS} \quad (2)$$

$$\ddot{q}_{SC} = M_{SC}^{-1}(f_{SC} + f_{dist} + f_{DF}) \quad (3)$$

$$a_{tmx} = m_{TM}^{-1}\left[f_{TMx} + h_{IS}F_{SUS\phi} + K_{xx}x_{tm} + K_{x\phi}\phi\right]. \quad (4)$$

The meaning of each symbol can be found in Table 1. The Eq. (4) is the measurement equation and x axis is the sensitive axis. The numerical values of the satellite and test mass parameters are displayed in Table 1, which are consistent with the values in (Antonucci et al. 2011). The stiffness, which is listed in Table 1, indicates that the design plant has unstable poles.

The disturbances acting on the test mass f_{tm} and the satellite f_{dist} are modeled as zero-mean Gaussian white noise shaped by low pass filters (Gath et al. 2004). The filters describing the different input disturbances are displayed in Fig. 2.

The position and attitude of the test mass are measured by GRS, and the measurement accuracy requirement is 2 nm/$\sqrt{\text{Hz}}$ in the displacement measurement, and 200 nrad/$\sqrt{\text{Hz}}$ in the rotation measurement, over the measurement bandwidth (Gath et al. 2004). The measurement noises are also modeled as zero-mean Gaussian white noises reshaped with low pass filters. The magnitude plots for the readout noise filters are shown in Fig. 3.

The thruster and the FEE are modeled as a first-order system in this study as follows:

$$\Gamma = \frac{\kappa}{\tau s + 1} \quad (5)$$

$$\Gamma_{FEE} = \frac{1}{\tau_{FEE} s + 1}. \quad (6)$$

As defined in (Pettazzi et al. 2009), an uncertainty of 50% with respect to the nominal value listed in Table 1 is considered on each element of the stiffness matrix. The scale factor κ indicates the static behavior of the thruster, which has an uncertainty of ±5%. An uncertainty of 50% is considered on the time constants of the thruster and FEE.

ADRC Based Drag-Free Design

Because of the uncertainty of the drag-free system and the coupling between the different coordinates, the design of the controller needs to take robustness and decoupling into account. As show in (Fichter et al. 2006) and (Pettazzi et al. 2009), the H_∞ and mixed structured singular value synthesis techniques have been proposed as methods to synthesize the SISO controllers. However, the structure of the controller is complex, and the control synthesis is conservative at the cost of the system performance. Therefore, this research is motivated by the problems that the parameters of the drag-free system are difficult to be obtained accurately, and coupling existed between different control loops. The goal of this research is to design decoupling controllers to suppress the uncertainty and disturbances of the drag-free satellite system.

In this work, a disturbance rejection based approach is proposed, where the cross-couplings between the drag-free loop and the suspension loop, as well as the external disturbances and internal uncertainties, are treated as "disturbance", which are estimated in real time and rejected. This disturbance decoupling control (DDC) strategy originates from a recently proposed novel control method referred as active disturbance rejection control (ADRC). The ADRC is a quite different design philosophy, with good robustness and simple structure. Therefore, the ADRC has promising potential in designing drag-free control laws. In this section, the design process is illustrated in the following subsections. In these subsections, first, we will define the performance specification for the drag-free system control design. Second, the active disturbance

Table 1 Variables and numerical of drag-free satellite

Parameter	Definition	Numerical value
$q=[x_{tm},\phi]$	General coordinates of the test mass	Variables
f_{SUS}	Electrostatic suspension generalized forces	Variable
F_{SUS}	Commanded suspensions forces	Variable
f_{TM}	Disturbance force directly acting on the proof mass	Variable
f_{dist}	External disturbance acting on the spacecraft	Variable
f_{SC}	Total force between the spacecraft and the test mass	Variable
f_{DF}	Force acting on the spacecraft due to the drag-free control	Variable
a_{tmx}	Acceleration of the test mass along the x axis	Variable
$M_q=diag(m_{TM}, I_{TM})$	General mass matrix of the test mass	1 kg, 6×10^{-4}kg·m^2
$K=\begin{bmatrix} K_{xx} & K_{x\phi} \\ K_{\phi x} & K_{\phi\phi} \end{bmatrix}$	Stiffness matrix between the test mass and satellite	$\begin{bmatrix} 2\times10^{-6}\frac{\mathrm{N}}{\mathrm{m}} & 0.003\times10^{-6}\frac{\mathrm{N}}{\mathrm{m}} \\ 0.006\times10^{-6}\mathrm{N} & 0.004\times10^{-6}\frac{\mathrm{N}}{\mathrm{m}} \end{bmatrix}$
$H_{IS}=\begin{bmatrix} 0 & h_{IS} \\ 0 & 0 \end{bmatrix}$	Actuation coupling matrix	$\begin{bmatrix} 0 & 0.5\frac{1}{\mathrm{m}} \\ 0 & 0 \end{bmatrix}$
M_{SC},I_{SC}	General mass matrix of the satellite	500 kg, 500 kg·m^2
κ	Scale factor of the thruster	1
τ	Time constant of the thruster	0.1303s
τ_{FEE}	Time constant of the FEE	0.065 s

rejection control strategy will be introduced, and the general form of ADRC for single input single output (SISO) system is given. Third, the internal model control structure of ADRC will be derived in this section, and the result of this section will be used in the robust stability verification for each control loop. Fourth, the idea of disturbance decoupling control is presented. Fifth, the details of design controllers for drag-free and suspension loop are given.

Specifications for Control Design

In this research, the control design is considered successful if the residual absolute acceleration acting on the test mass along the x direction is kept below (Fichter et al. 2005a):

$$S_y^{1/2}\leq 3\times10^{-14}\left[1+\left(\frac{f}{3\mathrm{mHz}}\right)^2\right]\frac{\mathrm{m}}{\mathrm{s}^2}\frac{1}{\sqrt{\mathrm{Hz}}} \tag{7}$$

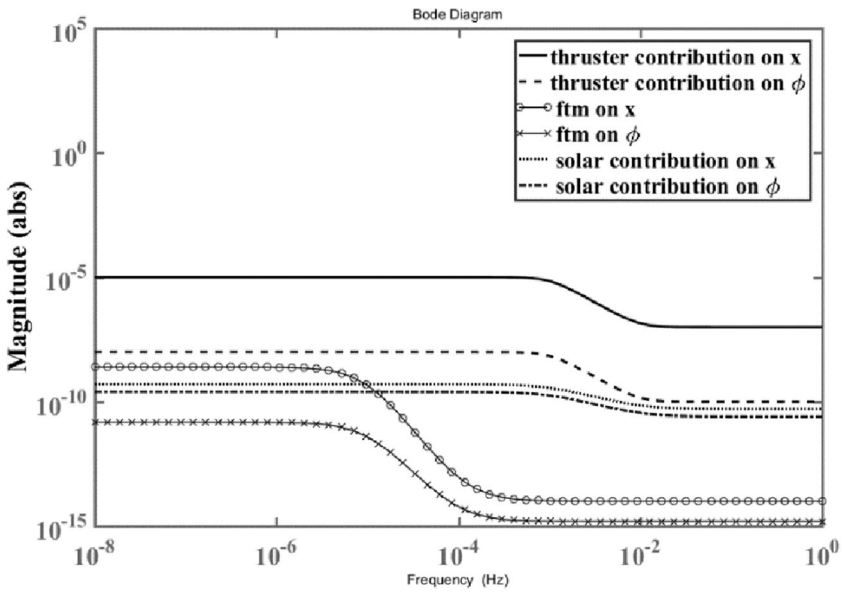

Fig. 2 Input disturbance weights. Disturbance force unit $\mathrm{N}/\sqrt{\mathrm{Hz}}$, and disturbance torque unit $\mathrm{N\cdot m}/\sqrt{\mathrm{Hz}}$

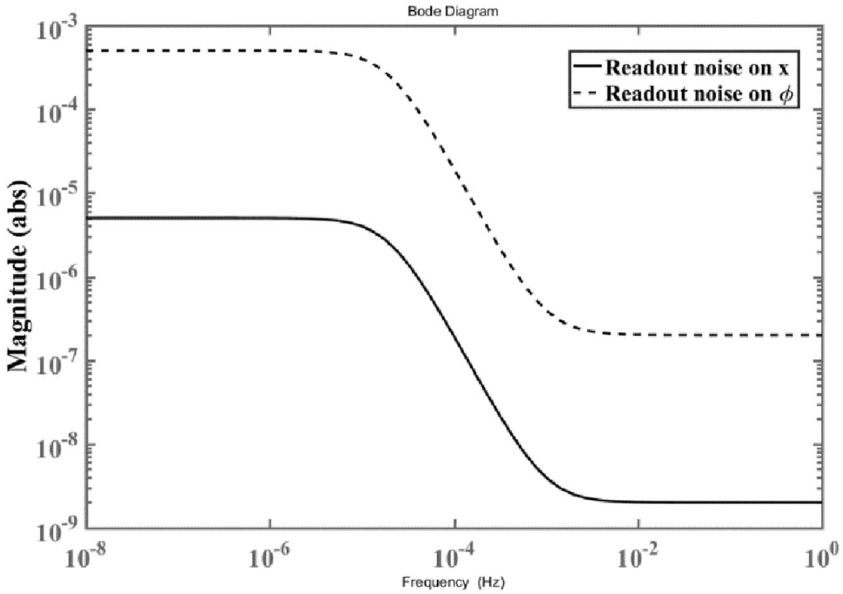

Fig. 3 Measurement noise weight. Unit for measurement noise on x is $\mathrm{m}/\sqrt{\mathrm{Hz}}$, and on ϕ is $\mathrm{rad}/\sqrt{\mathrm{Hz}}$

In the measurement bandwidth (MBW)

$1\mathrm{mHz} \le f \le 100\mathrm{mHz}$

A decentralized controller structure is assumed in the current research, where the test mass x position is fed back by means of the thruster actuation and this control loop is drag-free loop. In addition, the attitude error is fed back by the suspension actuation and this control loop is suspension loop.

Active Disturbance Rejection Control

In this subsection, the general form of the ADRC based on reduce order extend state observer (RESO) for the SISO system is presented. Consideration is given to following model:

$$y^{(n)}(t) = bu(t) + f(y(t), u(t), d(t)) \tag{8}$$

Where $y(t)$, $u(t)$ and $d(t)$ are output, input and disturbance of the system respectively, and $f(y, u, d)$ is a combination of the unknown dynamics and the external disturbance of the plant, which is denoted as generalized disturbance and assumed to be unknown in ADRC design. The parameter n is the relative order of the system and b is the gain of the cascade integral model.

In ADRC framework, the central idea is to estimate the unknown generalized disturbance $f(y, u, d)$. Assuming the 'generalized disturbance' as an addition state, the augment state space model of the system (8) is:

$$\begin{aligned} \dot{x} &= Ax + Bu + Eh \\ y &= Cx \end{aligned} \tag{9}$$

Where $x_1 = y$, $x_2 = \dot{y}$ and $h = \dot{f}$, C=[1, 0, …, 0] is $n+1$dimensional vector, and

$$A = \begin{bmatrix} 0 & 1 & & \\ \vdots & & \ddots & \\ 0 & & & 1 \\ 0 & \cdots & \cdots & 0 \end{bmatrix}_{(n+1)(n+1)}, B = \begin{bmatrix} 0 \\ 0 \\ \vdots \\ b \\ 0 \end{bmatrix}_{(n+1)\times 1}, E = \begin{bmatrix} 0 \\ 0 \\ \vdots \\ 0 \\ 1 \end{bmatrix}_{(n+1)\times 1} \tag{10}$$

Due to $y = x_1$ can be measured. Only the estimation of x_i, $i \ge 2$ is needed. The linear reduce order extend state observer (RESO) (Xue and Huang 2013) is design as

$$\begin{aligned} \dot{\hat{z}} &= (A_e - LC_e)\hat{z} + (L_1 - \beta_1 L)y + B_e u \\ \hat{x} &= \hat{z} + Ly \end{aligned} \tag{11}$$

$$A_e = \begin{bmatrix} 0 & 1 & & \\ \vdots & & \ddots & \\ 0 & 0 & \cdots & 1 \\ 0 & \cdots & \cdots & 0 \end{bmatrix}_{n\times n}, B_e = \begin{bmatrix} 0 \\ 0 \\ \vdots \\ b \\ 0 \end{bmatrix}_{n}, \tag{12}$$

Where $\hat{x}$ is estimation of x except x_1, $\hat{z}$ is intermediate variable and $\hat{z} = [z_2 \ \cdots \ z_n \ z_{n+1}]$. L is the gain of the observer, and L_1 is intermediate variable.

$$L = [\beta_1 \quad \beta_2 \quad \cdots \quad \beta_n]^T \tag{13}$$

$$L_1 = [\beta_2 \quad \beta_3 \quad \cdots \quad \beta_n \quad 0]^T \tag{14}$$

$$C_e = [1 \quad 0 \quad \cdots \quad 0]_{1\times n} \tag{15}$$

When A_e-LC_e is asymptotically stable, $\hat{x}_2$, …, $\hat{x}_n$ will approximate y derivatives (up to order n-1), and $\hat{x}_{n+1}$ will approximate the generalized disturbance f. The control law will be chosen as

$$u = \frac{u_0 - \hat{x}_{n+1}}{b} \tag{16}$$

If the RESO is properly designed, i.e. $\hat{x}_{n+1} = f$. Reduce the origin system to an nth integral system

$$y^{(n)} = u_0 \tag{17}$$

The controller of system (17) can be design directly as a state feedback law:

$$u_0 = k_1\left(r - \hat{x}_1\right) + k_2\left(\dot{r} - \hat{x}_2\right) + \cdots + k_n\left(r^{(n)} - \hat{x}_n\right) \tag{18}$$

Where r is reference input, the observer gain L and feedback gain k_i can be tuned based on the bandwidth-parameterization method proposed by (Gao 2003). Assume the RESO poles are placed at ω_o and the closed-loop are placed at ω_c, such that the gain β_i and k_i are calculated as:

$$\beta_i = C_n^i \omega_o^i, i = 1, \cdots, n \tag{19}$$

$$k_i = C_n^{i-1} \omega_c^{n-i+1}, i = 1, \cdots, n \tag{20}$$

The final control law can be approximated as

$$\begin{aligned} u(t) &= \frac{k_1\left(r - \hat{x}_1\right) + k_2\left(\dot{r} - \hat{x}_2\right) + \cdots + k_n\left(r^{(n)} - \hat{x}_n\right) - \hat{x}_{n+1}}{b} \\ &= K_0\left(\hat{r} - \hat{x}\right) \end{aligned} \tag{21}$$

Where $K_0 = \begin{bmatrix} k_1 & k_2 & \cdots & k_n & 1 \end{bmatrix}/b$ and $\hat{r} = \begin{bmatrix} r & \dot{r} & \cdots & r^{(n-1)} & 0 \end{bmatrix}^T$. It can be seen that an ADRC is a general control structure that only need the relative order and the high frequency gain 'b'. It does not need to know the detailed structure and the parameters of the model. Based on the bandwidth-parameterization method the ADRC can be tuned with two parameters (ω_c andω_o). The general structure of ADRC is displayed in Fig. 4.

Internal Model Control Structure of ADRC

In this subsection, the internal model control structure of LADRC will be derived. This structure will be used in robust stability analysis of the drag-free system. By taking Laplace transform of (11), we have

$$s\hat{Z}(s) = (A_e - LC_e)\hat{Z}(s) + (L_1 - \beta_1 L)Y(s) + B_e U(s) \tag{22}$$

$$\hat{X}(s) = \hat{Z}(s) + LY(s) \tag{23}$$

Where $\hat{Z}(s)$ and $\hat{X}(s)$ is the Laplace transform of $z(t)$ and $x(t)$. $\hat{R}(s)$ is Laplace transform of $\hat{r}(t)$.

$$\hat{R}(s) = \begin{bmatrix} 1 & s & s^2 & \cdots & s^n & 0 \end{bmatrix}^T R(s) \tag{24}$$

Solve for$\hat{X}(s)$, and substitute it into $U(s) = K\left(\hat{R}(s) - \hat{X}(s)\right)$

$$\hat{X}(s) = \begin{pmatrix} 1 \\ s(sI - (A_e - LC_e))^{-1}L \end{pmatrix} Y(s) + \begin{pmatrix} 0 \\ (sI - (A_e - LC_e))^{-1}B \end{pmatrix} U(s) \tag{25}$$

$$U(s) = C_1(s)F_r(s)R(s) - C_2(s)Y(s) \tag{26}$$

Where

$$C_1(s) = \frac{1}{1 + K\begin{pmatrix} 0 \\ MB \end{pmatrix}}, C_2(s) = \frac{K\begin{pmatrix} 1 \\ sML \end{pmatrix}}{1 + K\begin{pmatrix} 0 \\ MB \end{pmatrix}} \tag{27}$$

$$M = (sI - (A_e - LC_e))^{-1} \tag{28}$$

And $F_r(s) = K\begin{bmatrix} 1 & s & s^2 & \cdots & s^n & 0 \end{bmatrix}^T$ .The conventional feedback structure shown in Fig. 5a, in drag-free control the set point $\boldsymbol{r} = 0$, such that the structure can be simplify as Fig. 5b. The above result shows that an ADRC is equivalent to a two-degree-of-freedom (TDF) feedback control structure shown in Fig. 5c.

In the TDF-IMC structure, we have

$$P_0 = \frac{b}{s^n} \tag{29}$$

$$U(s) = \frac{Q}{1 - P_0 Q Q_d} R(s) - \frac{Q Q_d}{1 - P_0 Q Q_d} Y(s) \tag{30}$$

Compared with (26), solving for Q and Q_d,

$$Q_d = \frac{C_2}{C_1 F_r}, Q = \frac{C_1 F_r}{1 + P_0 C_2} \tag{31}$$

And the sensitivity and complementary sensitivity functions

$$S = \frac{1 - Q P_0 Q_d}{1 + Q(P - P_0)Q_d}, T = \frac{Q P Q_d}{1 + Q(P - P_0)Q_d} \tag{32}$$

Assume P=P$_0$,the complementary sensitivity functions can be simplify as

$$T = P_0 Q Q_d \tag{33}$$

By the small-gain theorem, a sufficient condition for the system stable is

$$|T\Delta|_\infty < 1 \tag{34}$$

Δ is multiplicative perturbation of the system. Substitute (34) into (33), the sufficient condition for the system stable is

$$|Q(j\omega)Q_d(j\omega)| < \frac{1}{|P(j\omega) - P_0(j\omega)|} \tag{35}$$

The formula (35) is the robust stability condition of ADRC control for SISO system.

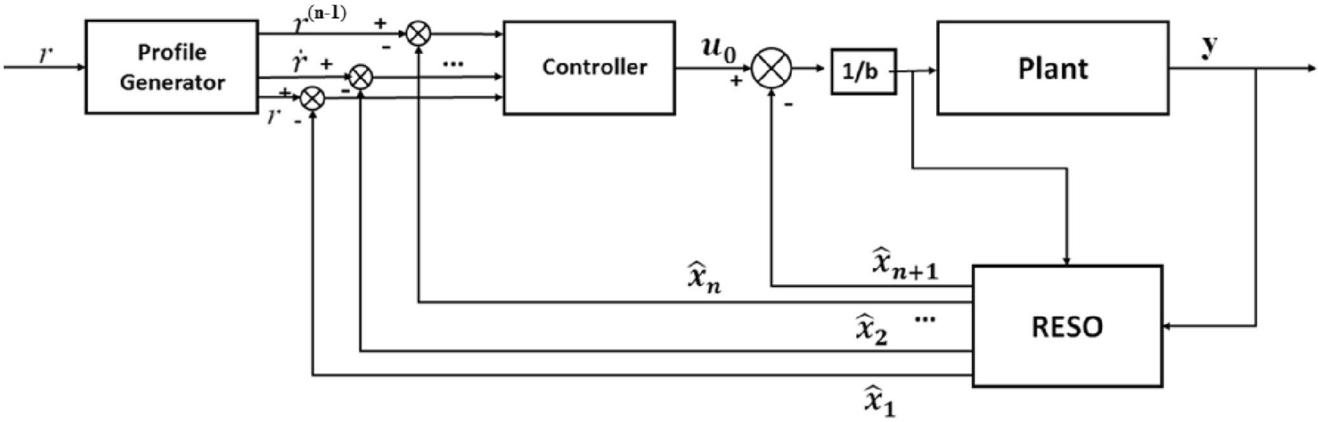

Fig. 4 the general structure of ADRC

Disturbance Decoupling Control

In section B and C, the ADRC for SISO system is addressed. However, the problem encountered in this paper is about multi-input multi-output system. In this paper, an ADRC based DDC approach is proposed to address the decoupling problem for the drag-free systems. The cross-couplings between the control loops, as well as the external disturbances, are treated as "disturbance". An ESO is designed for each control loop, and the state and disturbances are estimated in real time by the ESO. On the other hand, a control law is designed based on the estimation similar to section B. The DDC is briefly addressed in the following section. Let:

$$\begin{aligned}
\theta_1 &= \left[y_1^{(n_1-1)}(t), y_1^{(n_1-2)}(t), ..., y_1(t)\right] \\
\theta_2 &= \left[y_2^{(n_2-1)}(t), y_2^{(n_2-2)}(t), ..., y_2(t)\right] \\
&\vdots \\
\theta_m &= \left[y_m^{(n_m-1)}(t), y_m^{(n_m-2)}(t), ..., y_m(t)\right] \\
u &= [u_1(t), u_2(t), \cdots, u_m(t)] \\
w &= [w_1(t), w_2(t), \cdots, w_m(t)]
\end{aligned} \tag{36}$$

Then, by considering a system formed by a set of coupled input and output equations with predetermined input and output parings:

$$\begin{cases}
y_1^{(n_1)} = f_1(\theta_1, \theta_2, \theta_m, \cdots, w, u, t) + b_{11}u_1 \\
y_2^{(n_2)} = f_2(\theta_1, \theta_2, \theta_m, \cdots, w, u, t) + b_{22}u_2 \\
\qquad\qquad\vdots \\
y_m^{(n_m)} = f_m(\theta_1, \theta_2, \theta_m, \cdots, w, u, t) + b_{mm}u_m
\end{cases} \tag{37}$$

Where y_i is the output, u_i is the input, and w_i is the external disturbances of the ith loop; $y_i^{(n)}$ denotes the n_ith order derivative of y_i, $i = 1, 2, 3, \ldots,$ m; and f_i represents the combined effect of the internal dynamics and external disturbances in the ith loop, including the cross-channel interference. It should be noted that i refers to $i = 1, 2, 3\ldots,$ m in the following. In (37), it is assumed that the numbers of inputs and outputs are the same, and the order n_i and input gain b_{ii} are obtained. Next for the ith loop, an n_ith-order ADRC controller can be design to make y_i follow reference signal of the i th loop. In ADRC controller for every loop, f_i is estimated and compensated by ESO, and the state feedback controller is design the same as the SISO system. The structure of DDC is show in Fig. 6.

Combine ADRC and DDC to Solve Drag-Free Control

The methods presented in section B, C, and D are combined to solve the drag-free control problem. The system Eq. (1) is divided into two parts. The first is the plant of the x_{tm} direction, and its total disturbance. The second is the plant of the suspension loop, and its total disturbance. With the disturbance decoupling control, it could be assumed that the total disturbances in each loop are rejected by the control. Therefore, the measurement Eq. (4) could be represented by the sensitivity and complementary sensitivity function of each of the control loops.

In this section DDC is applied to control drag-free system.

First, the transfer function of the x_{tm} direction is derived from Eq. (1) as follows:

$$\begin{aligned}
m_{tm}\ddot{x}_{tm} &= k_{xx}x_{tm} + k_{x\phi}\phi + h_{IS}F^{IS}{}_{SUS} + f_{tm_x} \\
&\quad + b_{11}(f_{dist_x} + f_{DF})b_{11} = -\frac{m_{tm}}{m_{SC}}
\end{aligned} \tag{38}$$

$$b_{11} = -\frac{m_{tm}}{m_{SC}}$$

Then, by assuming:

$$f_1 = k_{x\phi}\phi + h_{IS}F_{SUS} + f_{tm\_x} + b_{11}f_{dist\_x} \tag{39}$$

Along with $d_{DF} = f_1/b_{11}$, such that:

$$\ddot{x}_{tm} = \frac{k_{xx}}{m_{tm}}x_{tm} + \frac{b_{11}(u_1 + d_{DF})}{m_{tm}} \tag{40}$$

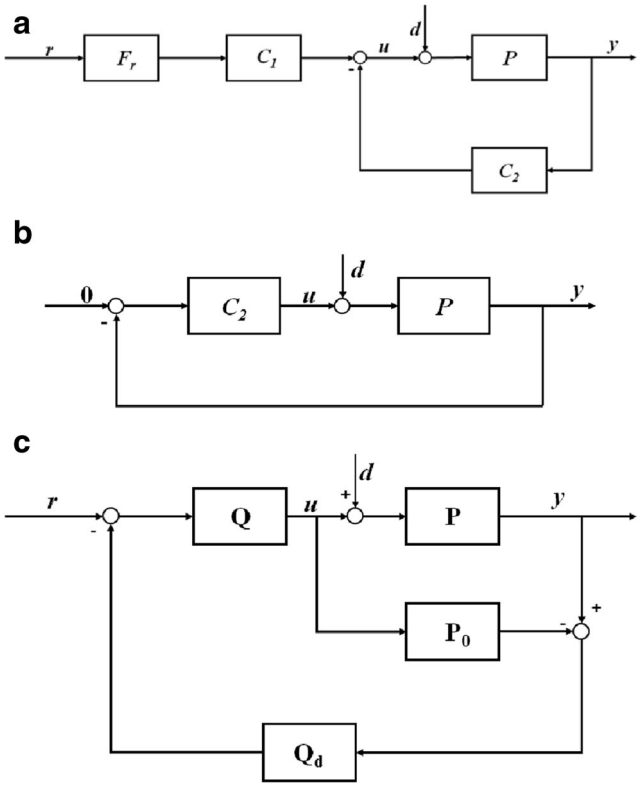

Fig. 5 **a** the general structure of ADRC. **b** ADRC for drag-free satellite. **c** the two-degree-of-freedom IMC

Then, this equation is converted into frequency domain using the Laplace transform, the plant transfer function is:

$$G_{DF} = \frac{b_1}{s^2 - K_x} \tag{41}$$

Where $b_1 = b_{11}/m_{tm}$, and $K_x = k_{xx}/m_{tm}$. Similarly, the plant transfer function of the suspension loop is:

$$G_{SUS} = \frac{b_2}{s^2 - K_\phi} \tag{42}$$

Where $b_2 = 1/I_{\mathrm{tm}}$, and $K_\phi = k_{\phi\phi}/I_{tm}$, and the disturbance of the suspension loop is as follows:

$$\begin{aligned} f_2 &= k_{\phi x} x_{tm} + f_{tm\_\phi} + b_{22} f_{dist\_\phi} \\ b_{22} &= -\frac{I_{tm}}{I_{SC}} \end{aligned} \tag{43}$$

In this model, the coupling terms in Eq. (34) $k_{x\phi}\phi + h_{IS}F_{sus}$ and (38) $k_{\phi x}x_{tm}$ are treated as external disturbances. In addition, f_1 and f_2 are estimated by the ESO of the drag-free and suspension loops and cancelled by the PD controller stated in Eq. (18). Finally, the full control structure of the drag-free and suspension loops could be constructed, as shown in Fig. 7. As derived in (27), the controllers G_{C_DF} and G_{C_SUS} can be expressed as

$$C_2(s) = G_c(s) = \frac{1}{b}\frac{C_{n2}s^2 + C_{n1}s + C_{n0}}{C_{d2}s^2 + C_{d1}s} \tag{44}$$

Where the coefficient can be found in the appendix. The two controllers have the same structure, the differences lies in choosing extend state observer bandwidth ω_o and controller bandwidth ω_c.

The closed loop expressions of each of the two loops could be derived, which are substituted into Eq. (4) as follows:

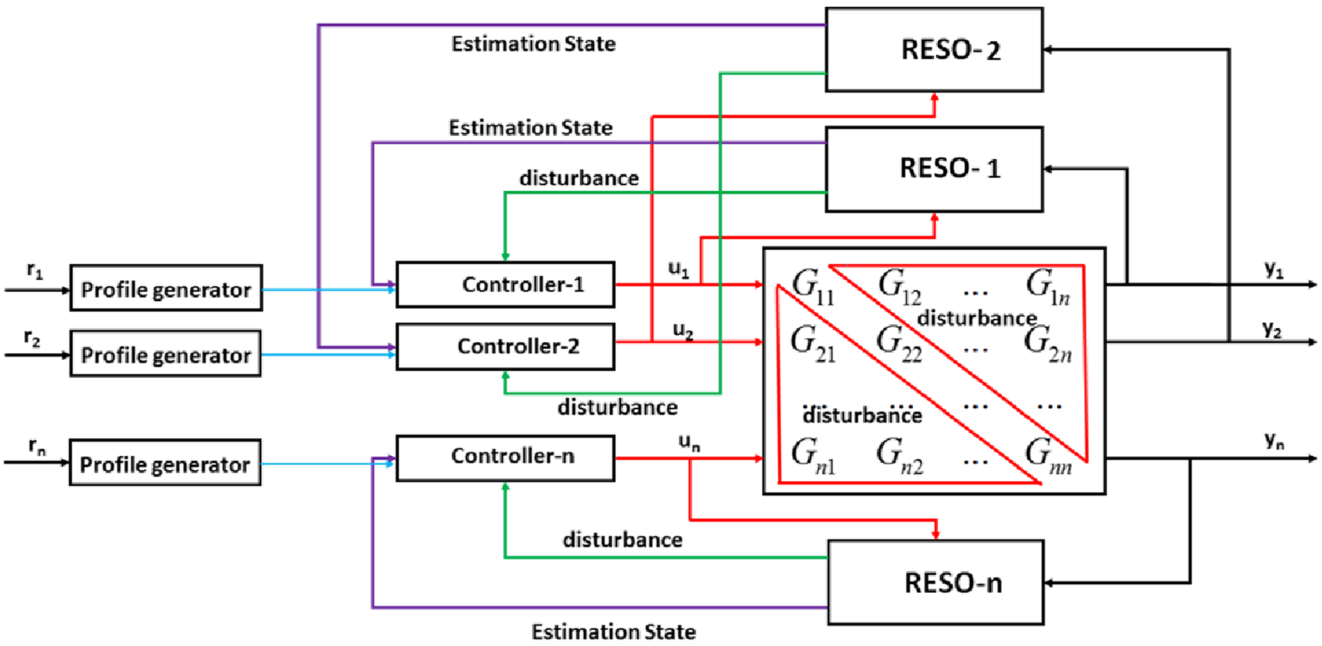

Fig. 6 the structure of disturbance decoupling control based on ADRC

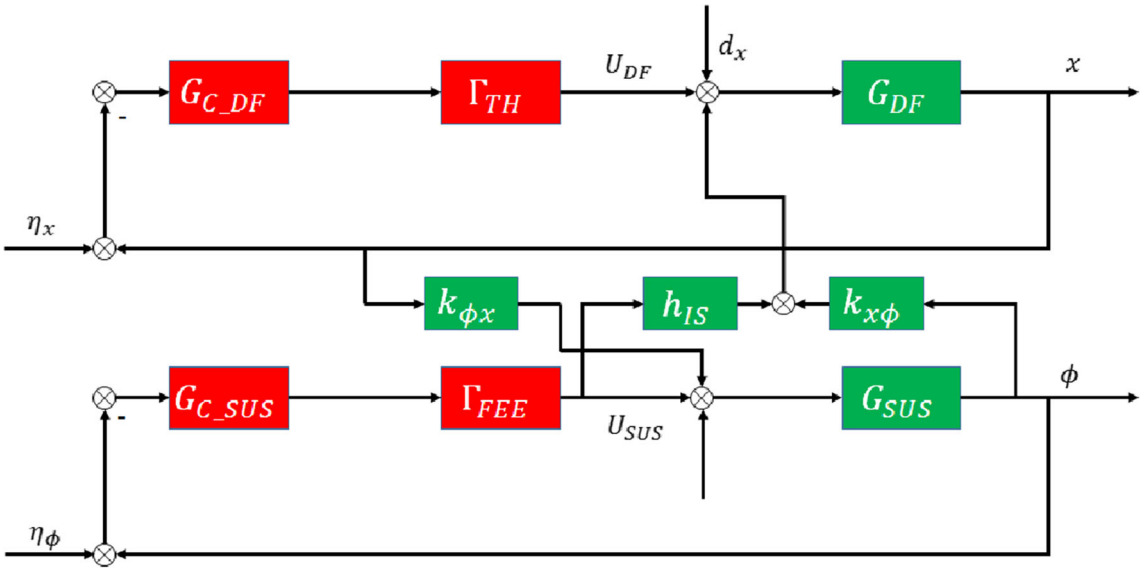

Fig. 7 Block diagram of the drag-free satellite system

$$a_{tmx}(s) = m_{tm}^{-1}\left\{f_{tm\_x} + k_{xx}[S_{DF}G_{DF}d_{DF} - T_{DF}\eta_x] + k_{x\phi}[S_{SUS}G_{SUS}f_2 - T_{SUS}\eta_\phi] + h_{IS}\left[-T_{SUS}f_2 - T_{sus}\eta_\phi/G_{SUS}\right]\right\} \tag{45}$$

Where the sensitivity and complementary sensitivity functions

$$S_{DF} = \frac{1}{1 + G_{C\_DF}\Gamma G_{DF}}, T_{DF} = \frac{G_{C\_DF}\Gamma_{TH}G_{DF}}{1 + G_{C\_DF}\Gamma G_{DF}} \tag{46}$$

$$S_{SUS} = \frac{1}{1 + G_{C\_SUS}\Gamma_{FEE}G_{SUS}}, T_{SUS} = \frac{G_{C\_SUS}\Gamma_{FEE}G_{SUS}}{1 + G_{C\_SUS}\Gamma_{FEE}G_{SUS}} \tag{47}$$

From the closed loop measurement relation in Eq. (45), the top level required in Eq. (7) is broken down into specifications on the drag-free and suspension loops, respectively. Those specifications, which are given in the MBW, are shown in Table 2.

Design Result

Search Program for Parameters Stable and Performance Region

The parameter setting method of ω_o and ω_c is presented in this section. There are two points which are taken into consideration. On one hand, the closed loop should be stable. On the other hand, the closed performance requirements shown in Table 2 should be met.

The stabilities of the drag-free and suspension loops are determined by the pole location of (46) and (47), in which the characteristic polynomials of the drag-free and suspension loops are as follows:

$$A_{df}(s) = A_5s^5 + A_4s^4 + A_3s^3 + A_2s^2 + A_1s + A_0 \tag{48}$$

$$B_{sus}(s) = B_5s^5 + B_4s^4 + B_3s^3 + B_2s^2 + B_1s + B_0 \tag{49}$$

The coefficients of A_{df} and B_{sus} have the same form, so we only give the coefficients of A_{df} in appendix. Usually, Routh-Hurwitz criterion is used to derive inequality relation between ω_o and ω_c for the stable region of the closed-loop system. However, it is complex for a fifth order characteristic polynomial. A search program is used to determine the region in ω_o-ω_c plane where the closed loop system is stable. The procedure of searching parameters stability region for drag-free and suspension loop is as following:

Step 1: Input parameters of drag-free loop or suspension loop, search region for ω_o-ω_c, search step length.
Step 2: For every ω_o-ω_c in search region, compute C_{n2} C_{n1} C_{n0} C_{d1} C_{d0}, compute the coefficients of A_{df} and B_{sus}, compute the roots of the characteristic polynomial, and then the real part of the roots.
Step 3: If max value of the real part <0, store the ω_o-ω_c.
Step 4: Output all ω_o-ω_c satisfy the stability condition.

Table 2 Specification on different control variable

Variable	Specification in the MBW
x_{tm}	$5 \times 10^{-9}\left[1 + \left(\frac{f}{3\text{mHz}}\right)^2\right]\frac{f}{3\text{mHz}}$
ϕ	$1.66\times10^{-6}\left[1 + \left(\frac{f}{3\text{mHz}}\right)^2\right]\frac{f}{3\text{mHz}}$
u_{SUS}	$3\times10^{-14}\left[1 + \left(\frac{f}{3\text{mHz}}\right)^2\right]\frac{f}{3\text{mHz}}$

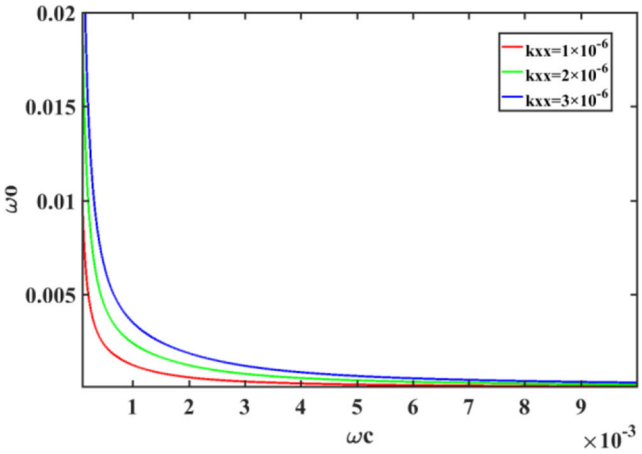

(a) Stable region for uncertainty in k_{xx}

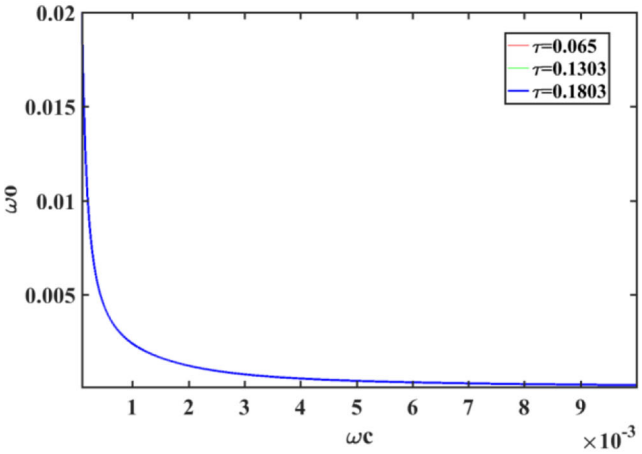

(b) Stable region for uncertainty in time constant τ

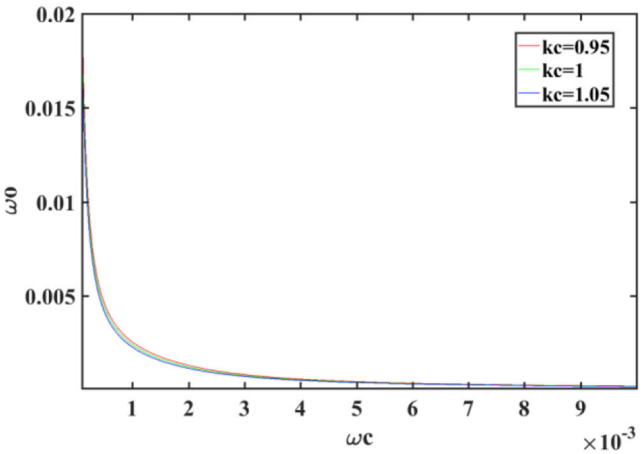

(c) The stable region for uncertainty in k_c

Fig. 8 the stable region ω_o-ω_c of drag-free loop. **a** Stable region for uncertainty in k_{xx}. **b** Stable region for uncertainty in time constant τ. **c** The stable region for uncertainty in k_c

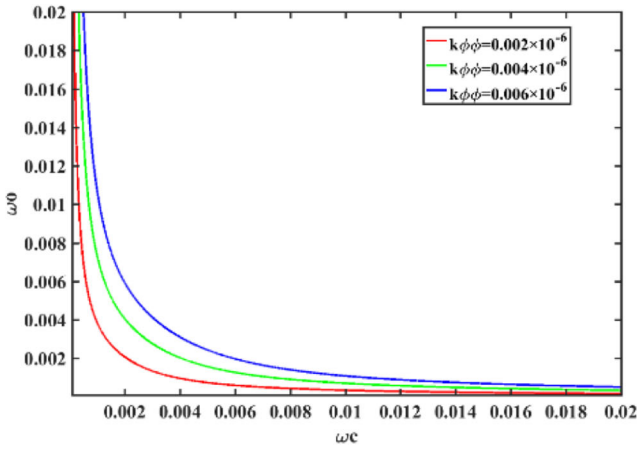

(a) The stable region for different $k_{\phi\phi}$

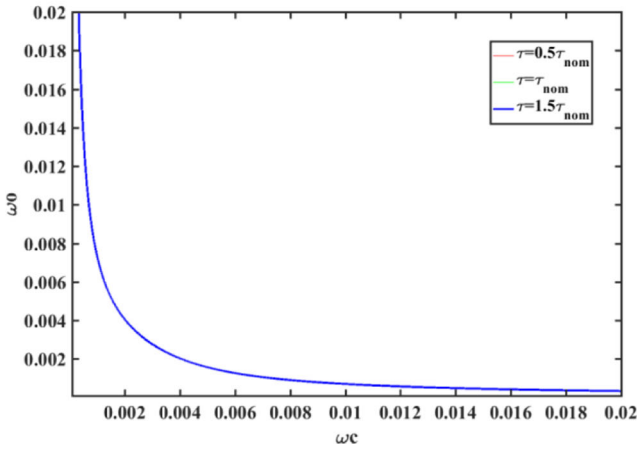

(b) Stable region for different time constant τ.

Fig. 9 the stable region ω_o-ω_c of suspension loop. **a** The stable region for different $k_{\phi\phi}$. **b** Stable region for different time constant τ

The results are shown in Figs. 8 and 9, where the area to the upper-right side of the curve is the stable region. Figure 8 shows that, even though the plant G_{DF} is unstable, the closed-loop system could be stable, given enough controller and observer bandwidth. It is also shown that the uncertain parameter k_{xx} has an impact on the stable region of ω_o - ω_c when the values of the ω_o - ω_c are closed in the region [0, 0.008]. However, as the ω_o- ω_c increase, the uncertainty of k_{xx} has little impact on the stability of the system. The impact on the stability of uncertainty of the thruster are detailed in Fig. 8b and c. In Fig. 8b, it can be seen that the stable region of the ω_o - ω_c is almost the same when the time constant τ varies. Also, the uncertainty of the scale factor k_c shows impacts on the stability of the system which are similar to that of k_{xx}. The stable region of the ω_o - ω_c for the suspension loop is shown in Fig. 9. Similar to k_{xx}, the uncertainty of $k_{\phi\phi}$ is found to impact the stability of this loop when the values of the ω_o - ω_c are

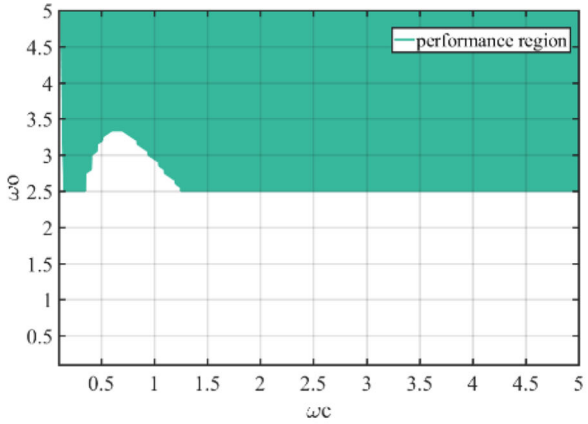

(a) The performance ω_o-ω_c region for drag-free loop

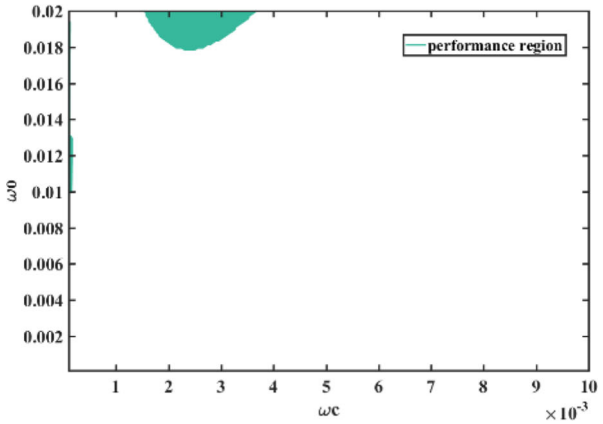

(b) The performance ω_o-ω_c region for drag-free loop for suspension loop

Fig. 10 The performance region for the system. **a** The performance ω_o-ω_c region for drag-free loop. **b** The performance ω_o-ω_c region for drag-free loop for suspension loop

closed in the region [0, 0.008]. Furthermore, the uncertainty of the time constant has very little impact on the stability of the suspension loop.

The closed-loop performance requirements of this system (Table 2) could be expressed as follows:

$$x_{tm} = S_{DF}G_{DF}d - T_{DF}\eta_x \tag{50}$$

$$\phi = S_{SUS}G_{SUS}d_{SUS} - T_{SUS}\eta_\phi \tag{51}$$

$$U_{SUS} = -T_{SUS}d_{SUS} - G_{C\_SUS}\eta_\phi/(1 + G_{C\_SUS}G_{SUS}) \tag{52}$$

Where d is the disturbance of the drag-free loop, and is the combination of the thruster noise and solar noise. The contributions of the coupling and stray force are discarded for simplicity. The d_{SUS} contains the stray force, as well as the thruster and solar noise contributions. On the other hand, in order to guarantee the robustness and stability margins, constraints are imposed on the sensitivity and complementary functions of each loop as follows:

$$S \leq 1.4125 T \leq 1.4125 \tag{53}$$

Then, using these relationships and requirements, a search program is established to determine the ω_o - ω_c for each loop. The procedure of searching parameters meeting the performance requirements is as following:

Step 1: Input the parameters of the drag-free or suspension loop, the search region of for ω_o-ω_c, and the search step length, the measurement bandwidth.
Step 2: Calculate the total disturbance on the drag-free loop d and on the suspension loop d_{SUS}.
Step 3: for every ω_o-ω_c in search region, calculate the controller G_c for each loop by Eq. (44), sensitivity and complementary sensitivity function for each loop by Eqs. (46) and (47).

Table 3 the controller parameters of each loop

Parameters	ω_o	ω_c
Drag-free loop	3.65	0.2
Suspension loop	0.02	0.002

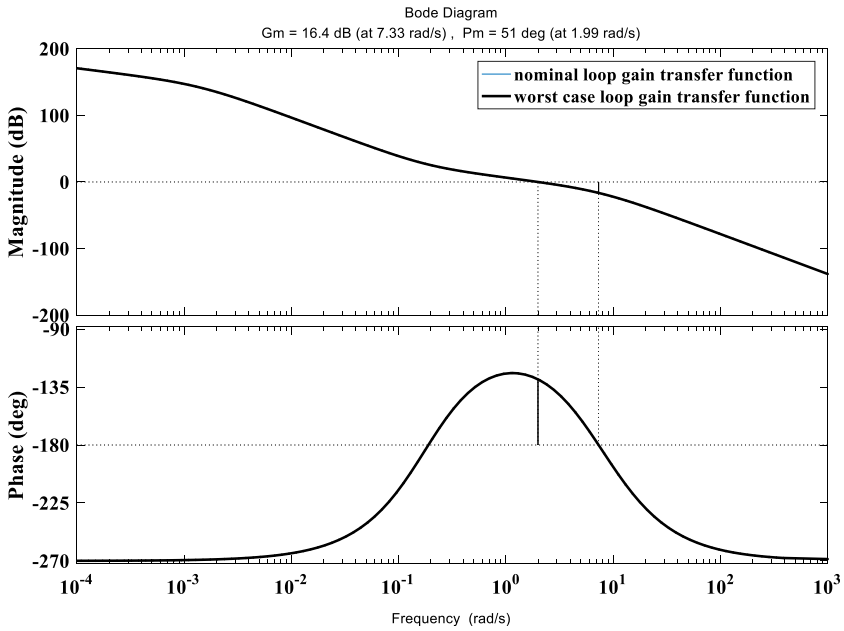

Fig. 11 The gain margin and phase margin of the drag-free loop

Step 4: Calculate $|x_{tm}(j\omega)|$, $|\phi(j\omega)|$ and $|u_{SUS}(j\omega)|$ by Eq. (50) (51) and (52) in measurement bandwidth.
Step 5: If the max value of $|x_{tm}(j\omega)|$, $|\phi(j\omega)|$ and $|u_{SUS}(j\omega)|$ < the specification in Table 2, store ω_o-ω_c.
Step 6: Output all ω_o-ω_c satisfy the performance requirements condition.

The performance region is shown in following figures. As detailed in Fig. 10, there are large amounts of the ω_o - ω_c which met the requirements. The parameters choosing for the controllers are shown in Table 3.

The Performance of Drag-Free Loop

The design results of the drag-free loop are presented in this section. First, the loop gain transfer function is $G_{C\_DF}\Gamma G_{DF}$, the bode plots of which are shown in Fig. 11. As can be seen in the figure, the nominal loop gain transfer function curve coincides with the worst-case loop gain transfer function. This indicates the uncertainty of the thruster and the system has little impact on the stability of the drag-free loop. The gain margin of this loop is determined to be 16.4 dB at 7.33 rad/s, and the

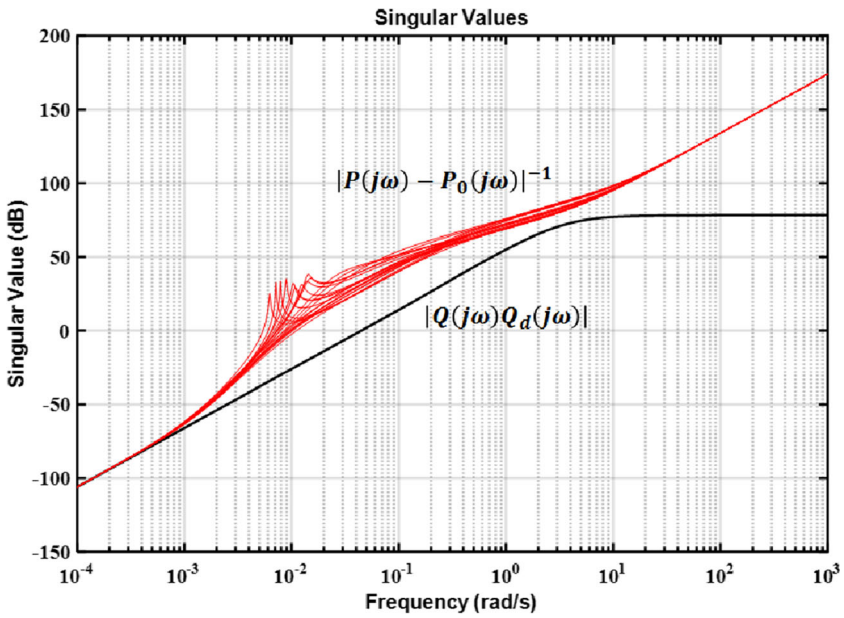

Fig. 12 singular value plot of the model uncertainty and the design controller for drag-free loop

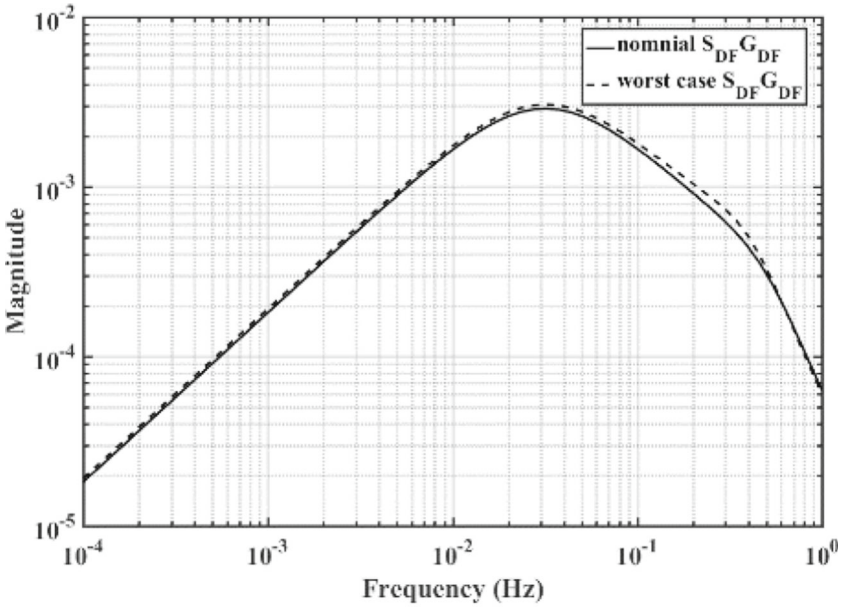

(a) $S_{DF}G_{DF}$ plot of the drag-free loop

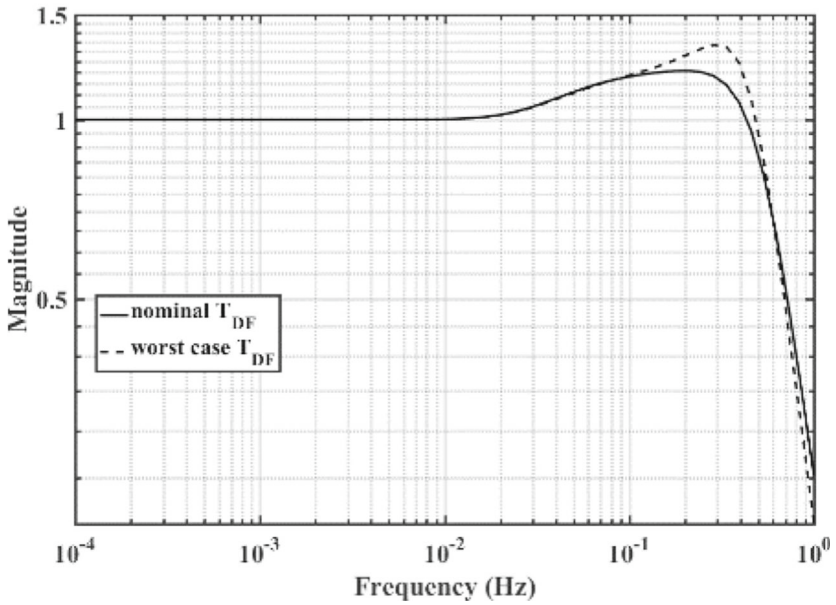

(b) T_{DF} plot of drag-free loop

Fig. 13 The $S_{DF}G_{DF}$ and T_{DF} and their worst-case plots. **a** $S_{DF}G_{DF}$ plot of the drag-free loop. **b** T_{DF} plot of drag-free loop

phase margin of this loop is 51 degrees at 1.99 rad/s. These results confirmed that the system has an exceptional stability margin. The plot of the design controller of the drag-free loop $|QQ_d|$ and the reciprocal of the model uncertainty $|P-P_0|$ are shown in Fig. 12. It is clear that $|QQ_d|<|P-P_0|$. So with the chosen parameters, the drag-free loop is robust stable.

Second, the system's performance in regard to suppressing disturbances and noise are shown in Fig. 13a. The bode plots of the nominal $S_{DF}G_{DF}$, as well as the worst case $S_{DF}G_{DF}$ are shown in the figure. It is clear in the figure that the plots shows little difference throughout the entire frequency domain. In the MBW, the value of $S_{DF}G_{DF}$ is found to be close to 10^{-3}. These findings indicates that the controller has a good performance

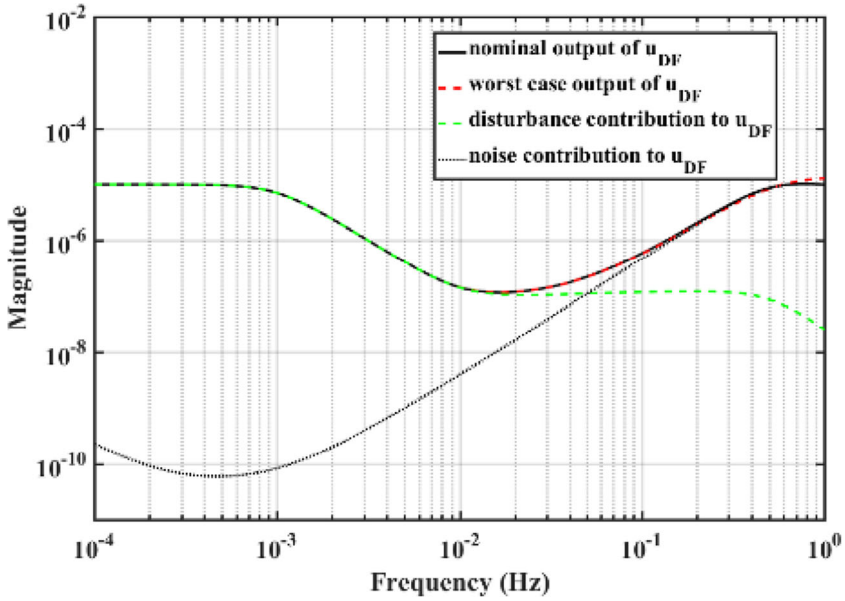

Fig. 14 The control signal output of drag-free loop

in disturbance suppressing. The bode plots of the nominal T_{DF} and worst case T_{DF} are illustrated in Fig. 13b. The uncertainty only shows the impacts on T_{DF} above 0.1 Hz. Also, the value of the T_{DF} is approximately 1, which indicates that the x output of this control loop is mainly from the measurement noise.

Third, the control output of the drag-free loop is shown in Fig. 14. In the figure, the black line indicates the nominal output of the controller output, and the red dotted line denotes the worst-case control output. This also indicates the uncertainty of the system's impact on the control output. The green dotted line and the black dotted line indicate the contributions on the control output. In the low frequency range $[10^{-4}, 10^{-2}]$, the control output is mainly from cancelling the disturbances, and in the relatively high frequency range, the control output is mainly from suppressing the noise.

Finally, the closed loop response of the drag-free system is shown in Fig. 15. The response results indicate that the controller could meet the requirement, since the disturbances acting on the drag-free loop are largely suppressed.

The Performance of Suspension Loop

In this section, the design result of suspension loop is presented. Figure 16 details the nominal S_{SUS} and T_{SUS}, as well as the

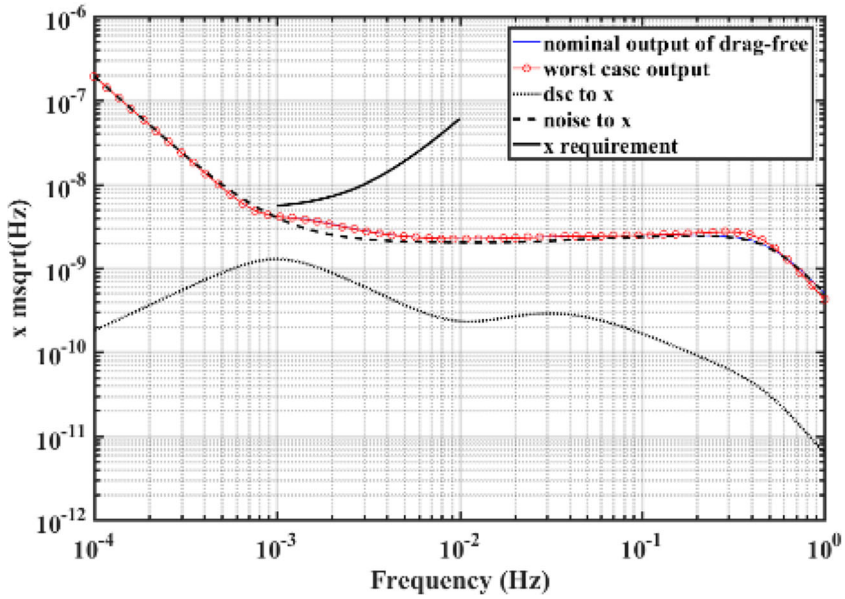

Fig. 15 The closed loop response of the drag-free loop

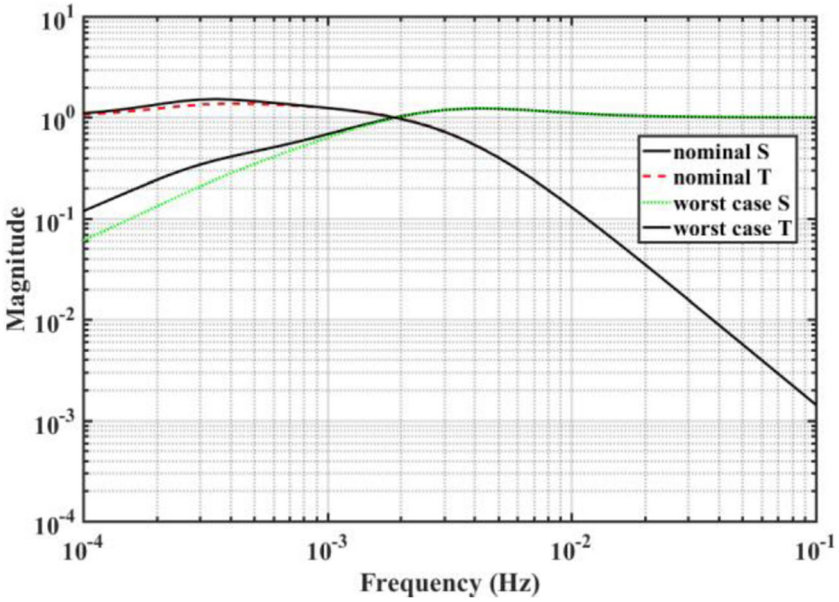

Fig. 16 Sensitivity function and complementary sensitivity function of the suspension loop

worst-case S_{SUS} and T_{SUS} of the suspension loop. The uncertainty of system is found to affect the sensitivity and complementary sensitivity functions in the low frequency range below 10^{-3} Hz.

Figure 17 shows the Bode plot of the loop gain transfer function $G_{C\_SUS}\Gamma_{FEE}G_{SUS}$ that has a negative gain margin of −12.3 dB at 0.00175 rad/s, and the phase margin of this system is 59.8 degrees at 0.012 rad/s. The uncertainty of this loop is determined to have little effect on the stability margin. As shown in Section III C. The plot of the design controller of suspension loop $|QQ_d|$ and the reciprocal of the model uncertainty $|P-P_0|$ are shown in Fig. 18. It is clear that $|QQ_d|<|P-P_0|$. So with the chosen parameters, the suspension loop is robust stable.

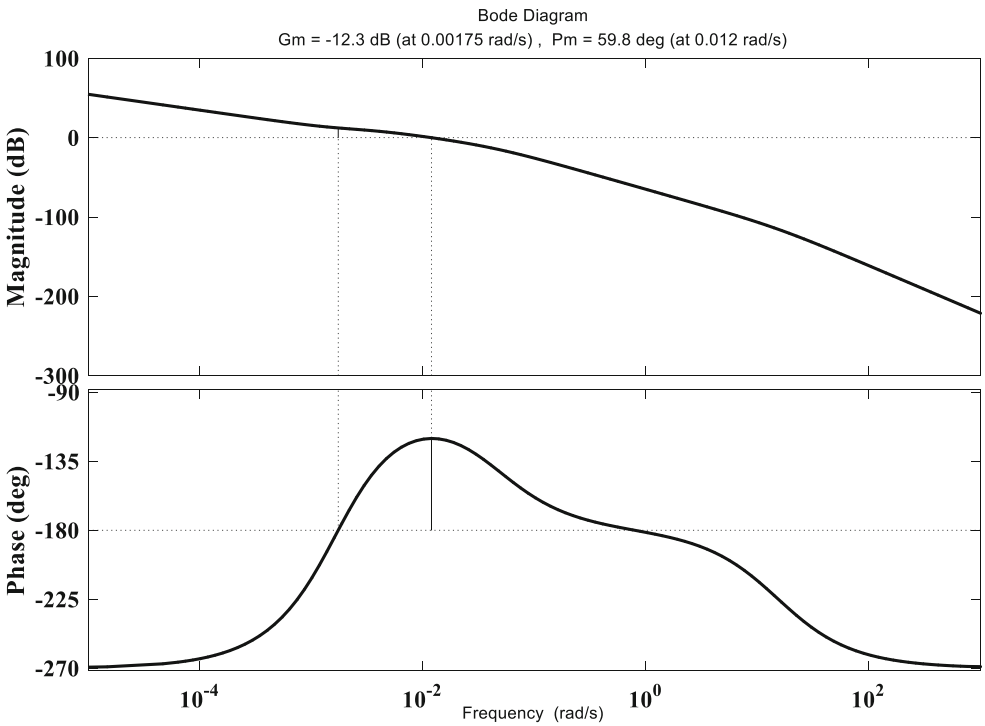

Fig. 17 The loop gain transfer function of the suspension loop

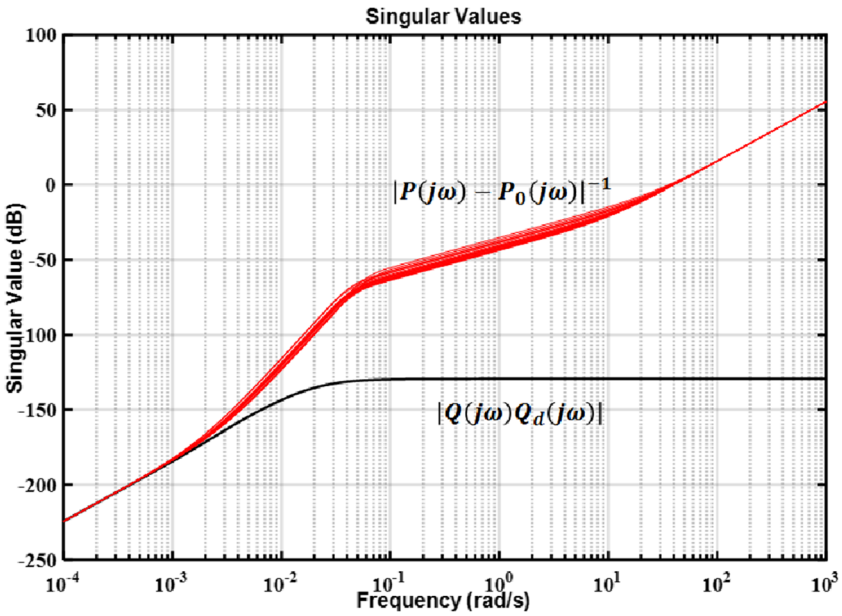

Fig. 18 singular value plot of the model uncertainty and the design controller for suspension loop

The control output of the suspension loop is shown in Fig. 19. The black line indicates the nominal output of the controller output, and the black dotted line shows the worst-case control output. Also, the uncertainty of the system's impact on the control output is presented. This figure also presents the contributions of the disturbances and measurement noise on the control output. The results indicates that the requirements on control output U_{SUS} are met. The closed-loop output of the suspension loop is shown in Fig. 20. The original impacts from the disturbances and noise are also presented in this figure, and the requirements on ϕ are also met by the controller.

The Simulation Result

In Section III C, the coupling of different coordinates is not taken into consideration in design parameters of the controller. Therefore, the controller performance is checked posteriori. In this section, the simulation of the overall system is implemented. Figure 21 shows the results of this simulation. The black line in the figure indicates the residual acceleration on the test mass, and the red line shows the top requirement on the system. It can be seen in this figure that the controller meets the top requirement. Also in this figure, the major source of the

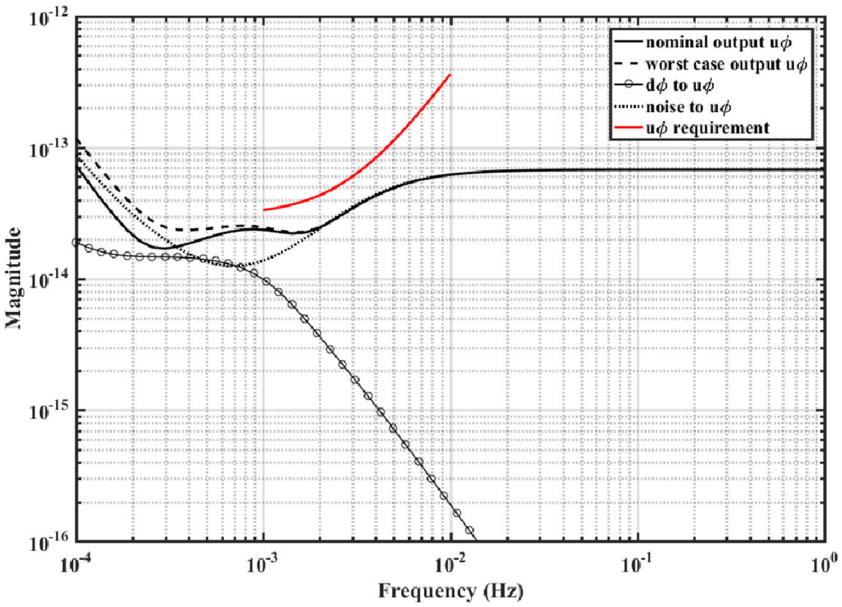

Fig. 19 The control signal of the suspension loop

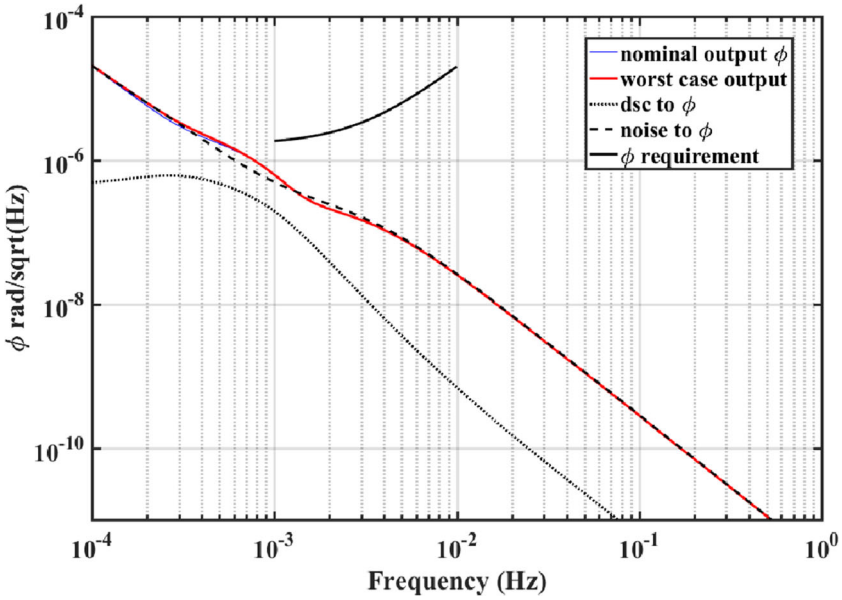

Fig. 20 The output of ϕ of the suspension loop

residual acceleration of the test mass is the electrostatic actuation cross talk $H_{IS}F_{SUS}$, which is denoted by the magenta line. The contributions of the stiffness coupling of x and ϕ are largely suppressive, as shown by the green and blue lines.

Conclusion

This research addresses the problem of the design of an active disturbance rejection controller for a high accuracy drag-free satellite with a cubic test mass. First, the uncertain model of the drag-free satellite is defined. The performance requirement imposed on the acceleration of the test mass are broken down into the specifications of the drag-free and suspension loops, due to the disturbance decoupling controller. The parameter stability, along with the regions of the controller which satisfies the performance requirements, are determined using a search program. The design technique is found to be robust for the perturbation of the system, and displays strong performance in suppressing the disturbances. Then, in order to check the design of the controller, an overall simulation is performed. The results confirms that the controller could meet the top requirement.

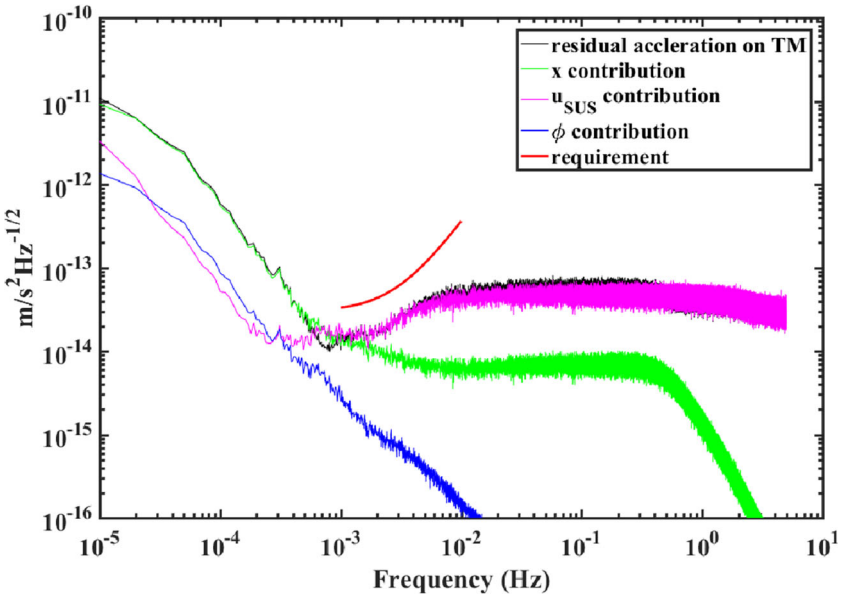

Fig. 21 The simulation result of overall system

Acknowledgments This work is supported by the Strategic Priority Research Program of the Chinese Academy of Sciences(Grant No.XDB23030100) and the National Natural Science Foundation of China (No.11372328). The author would like to thank the editor and reviewers for their valuable comments and constructive suggestions that helped to improve this paper.

Appendix

The coefficients in *C(s)* and *A(s)*, the coefficients of *B(s)* is the same as *A(s)*, so they are omitted.

$\mathrm{Cn2} = \omega o2 + 4\omega o\omega c + \omega c2$	$\mathrm{Cn1} = 2\omega c\omega o2 + 2\omega c2\omega o$
$\mathrm{Cn0} = \omega c2\omega o2$	$C_{d2} = 1$
$C_{d1} = 2\omega_c + 2\omega_o$	$C_{d0} = 0$
$A_5 = C_{d2}\tau$	$A_4 = C_{d2} + C_{d1}\tau$
$A_3 = C_{d1} - C_{d2}k_x\tau$	$A_2 = C_{n2} - C_{d2}k_x - C_{d1}k_x\tau$
$A_1 = C_{n1} - C_{d2}k_x$	$A_0 = C_{n0}$

References

Antonucci, F., Armano, M., et al.: From laboratory experiments to LISA Pathfinder: achieving LISA geodesic motion. Classical and Quantum Gravity. **28**(9), 094002 (2011). https://doi.org/10.1088/0264-9381/28/9/094002

Armano, M., et al.: Sub-Femto-g Free Fall for Space-Based Gravitational Wave Observatories: LISA Pathfinder Results. Phys. Rev. Lett. **116**, 231101 (2016). https://doi.org/10.1103/PhysRevLett.116.231101

Bortoluzzi, D., Da Lio, M., Dolesi, R., Weber, W., Vitale, S.: The LISA Technology Package Dynamics and Control. Classical and Quantum Gravity. **20**(10), S227–S238 (2003)

Bortoluzzi, D., Da Lio, M., Oboe, R., and Vitale, S.: Spacecraft High Precision Optimized Control for Free-Falling Test Mass Tracking in Lisa-Pathfinder Mission, Advanced Motion Control, IEEE, Piscataway, NJ, pp. 553–558 (2004). https://doi.org/10.1109/AMC.2004.1297928

Canuto, E.: Drag-Free and Attitude Control for the GOCE Satellite. Automatica. **44**(7), 1766–1780 (2008). https://doi.org/10.1016/j.automatica.11.023

Carraz, O., Siemes, C., Massotti, L., Haagmans, R., Silvestrin, P.: A spaceborne gravity gradiometer concept based on cold atom interferometers for measuring Earth's gravity field. Microgravity Science and Technology. **26**(3), 139–145 (2014)

Chapman, D., Zentgraf, M., and Jafry, R.: Drag-Free Control Design Including Attitude Transition for the STEP Mission, Proceedings of the 5th ESA International Conference on Spacecraft Guidance Navigation and Control, European Space Agency, Noordwijk, The Netherlands (2002)

DeBra, D.B.: Drag-Free Spacecraft as Platforms for Space Missions and Fundamental Physics. Classical and Quantum Gravity. **14**(6, Paper 1549), (1997). https://doi.org/10.1088/0264-9381/14/6/026

Fichter, W., Gath, P., Vitale, S., Bortoluzzi, D.: LISA Pathfinder drag-free control and system implications. Classical and Quantum Gravity. **22**(10), S139–S148 (2005a). https://doi.org/10.1088/0264-9381/22/10/002

Fichter, W., Schleicher, A., Szerdahelyia, L., Theil, S.: Drag-Free Control System for Frame Dragging Measurements Based on Cold Atom Interferometry. Acta Astronautica. **57**(10), 788–799 (2005b). https://doi.org/10.1016/j.actaastro.2005.03.070

Fichter, W., Schleicher, A., Vitale, S.: Drag-Free Control Design with Cubic Test Mass. In: Hansjorg, D. (ed.) Lasers, Clocks and Drag-Free, pp. 361–378. Springer, Heidelberg (2006)

Gao, Z.: Scaling and Parameterization Based Controller Tuning, Proc. of the 2003 American Control Conference, Vol. 6, Denver, pp. 4989 – 4996 (2003)

Gath, P., Fichter, W., Kersten, M., Schleicher, A.: Drag Free and Attitude Control System Design for the LISA Pathfinder Mission, AIAA Paper 2004-5430 (2004). https://doi.org/10.2514/6.2004-5430

Gollor, M., Franke, A.: Electric Propulsion Electronics Activities in Europe 2016, 52nd AIAA/SAE/ASEE Joint Propulsion Conference, Salt Lake City (2016). https://doi.org/10.2514/6.2016-5032

Han, J.: From PID to active disturbance rejection control. IEEE Trans. Ind. Electron. **56**(3), 900–906 (2009). https://doi.org/10.1109/TIE.2008.2011621

Lange, B.: The Drag-Free Satellite. AIAA J. **2**(9), 1590–1606 (1964). https://doi.org/10.2514/3.55086

Leitner, J., "Investigation of Drag-Free Control Technology for Earth Science Constellation Missions," NASA Earth Science Technology Office Final Study Report, Vol. 15 (2003)

Li, G., Mance, D., Zweifel, P.: Actuation to sensing crosstalk investigation in the inertial sensor front-end electronics of the laser interferometer space antenna pathfinder satellite. Sensors Actuators A Phys. **167**(2), 574–580 (2011). https://doi.org/10.1016/j.sna.2011.03.011

Li, Y., Luo, Z., Liu, H., Gao, R., Jin, G.: Laser Interferometer for Space Gravitational Waves Detection and Earth Gravity Mapping. Microgravity Science and Technology. 2008(10), 1–13 (2018)

Liu, H., Li, S.: Speed control for pmsm servo system using predictive functional control and extended state observer. IEEE Trans. Ind. Electron. **59**(2), 1171–1183 (2012). https://doi.org/10.1109/TIE.2011.2162217

Nguyen, A.N., Conklin, J.: Three-Axis Drag-Free Control and Drag Force Recovery of a Single-Thruster Small Satellite. J. Spacecr. Rocket. **52**(6), 1640–1650 (2015). https://doi.org/10.2514/1.A33190

Pettazzi, L. :Robust Controller Design for Drag-Free Satellites," Ph.D. Thesis, Faculty of Production Engineering, University of Bremen (2008)

Pettazzi, L., Lanzon, A., Theil, S., Finzi, E.A.: Design of Robust Drag-Free Controllers with Given Structure. J. Guid. Control. Dyn. **32**(5), 1609–1620 (2009). https://doi.org/10.2514/1.40279

Theil, S. :Satellite and Test Mass Dynamics Modeling and Observation for Drag-free Satellite Control of Step Mission," Ph.D. Thesis, Department of production Engineering University of Bremen, (2002)

Touboul, P., Foulon, B., Lafargue, L., Metris, G.: The microscope mission. Acta Astronautica. **50**(7), 433–443 (2002). https://doi.org/10.1016/S0094-5765(01)00188-6

Xia, Y., Zhu, Z., Fu, M., Wang, S.: Attitude Tracking of Rigid Spacecraft With Bounded Disturbances. IEEE Trans. Ind. Electron. **58**(2), 647–659 (2011). https://doi.org/10.1109/TIE.2010.2046611

Xue, W. Huang, Y.: On Frequency-domain Analysis of ADRC for Uncertain System, American Control Conference, Washington, DC, 6652-6657 (2013). https://doi.org/10.1109/ACC.2013.6580881

Zheng, Q., Chen, Z., Gao, Z.: A practical approach to disturbance decoupling control. Control. Eng. Pract. **17**(9), 1016–1025 (2009). https://doi.org/10.1016/j.conengprac.2009.03.005